INVESTIGATIONS ON PHYSICAL, MECHANICAL AND SLIDING WEAR ASSESSMENT OF ZA27-Gr ALLOY COMPOSITES USING PREFERENCE SELECTION INDEX METHOD

Ashiwani Kumar
Feroze Gandhi Institute of Engineering and Technology, Raebareli, U.P 229316, India

Mukesh Kumar
Malaviya National Institute of Technology, Jaipur, Rajasthan 302017, India

https://doi.org/10.1007/s40962-022-00953-z

Abstract

This present work investigates the physical, mechanical and sliding wear performance of graphite (0–6 wt%)-reinforced ZA-27 alloy composites following ASTM standards. Sliding wear experiments design follows the Taguchi methodology, and the same is adopted for parametric optimization. This follows surface micrograph studies using SEM to understand the associated wear mechanisms responsible for surface damage. Further, the compositions are ranked as per their performance criteria implications using Preference Selection Index (PSI) decision-making technique. It was observed that there are improvements in physical and mechanical properties like void content (2.50–1.33), hardness (107–171 HV), compressive strength (406–496 MPa) flexural strength (300–490 MPa), tensile strength (290–428 MPa) and impact strength (22.76–64 J), as well as sliding wear performance of alloy composites with reinforcement. The AGr-6 alloy composite having 6 wt% graphite particulates were observed to optimize the overall physical, mechanical, and sliding wear performance. The analysis of performance data using the PSI decision-making tool reveals AGr -6 >AGr -4 > AGr -2 > AGr -0 order of material composition that optimizes the required performance. As both decisions are attuned, decision-making tools like PSI could be used in such material selection problems.

Keywords: *ZA-27 alloy, graphite, sliding wear, alloy composites, mechanical properties, preference selection index method (PSI)*

Introduction

The zinc–aluminum alloy is a common monolithic substance used in industry. This kind of material is employed as bearing material because of its outstanding fluidity, castability, mechanical qualities, and wear resistance. Tribological characterizations are being taken into consideration for a variety of applications, including brakes for aircraft, pistons, cylinder liners, and lightweight materials.[1,2] A study of the mechanical characteristics of ZA-27 reinforced with SiC was conducted by Bhaskar Raju et al.[3] It was shown that increasing the reinforcement led to an improvement in the mechanical properties of composites, such as hardness, tensile strength, impact strength, and compressive strength. The strongest ceramic particles' influence on the base alloy matrix improves the mechanical characteristics. Dalmis et al.[4] studied the graphite nanoparticles addition on the mechanical and physical characterization of ZA-27 composites. According to reports, increasing the filler content decreased hardness and tensile strength. The ductile nature of Gr particles, which is easily plastically deformed of composites, and the strong connection between Gr particles and the base alloy matrix both contribute to an improvement in mechanical properties. Ranganath et al.[5] investigated the mechanical characterized and fractography of TiO_2-filled ZA-27 composites. It is observed that improvement in mechanical characterization as Young's modulus, ultimate tensile strength, yield strength, and hardness increases with an increase in the TiO_2. Short glass fibers' effects on the mechanical characteristics of the cast ZA-27 alloy composite were investigated by Sharma et al.[6] With increasing

Received: 05 October 2022 / Accepted: 30 December 2022 /
Published online: 23 January 2023

reinforcement, it has been found that the tensile strength, hardness, and Young's modulus all improve. Alaneme et al.[7] also examined the mechanical and wear behavior of steel chips-filled ZA-27 composites. It was found that hardness and wear resistance of the composites enhanced with enhancement in wt% of reinforcement. Girisha et al.[8] and Baradeswaran et al.[9] investigated the influences of graphite reinforced with ZA-27 alloy composites. It is found that the mechanical and tribological properties were improved with an increase in filler content. Guler et al.[10] studied the effect of nanoalumina content on corrosion behavior and microstructure of ZA27/graphite/alumina hybrid nanocomposites. It is observed that the corrosion behavior and microstructure of composite improve with the increase in reinforcement content. Similar outcomes are reported by Kumar et al.[11] and Kumar et al.[12] observed that the dry sliding wear performance improves with the increase in filler content. Huang et al.[13] observed that the tensile and fatigue behavior of composite performance improves with the enhancement in reinforcement content. Shariati et al.[14] found that the tensile and tribological properties improve with the increase in filler content. Kumar et al.[15] studied the influence of Al_2O_3/SiC on mechanical and tribological performance of AA2024 alloy composite and obtained the ranking performance of composite by using the PSI method. Similar findings are reported by various researchers[16,17] for mechanical and sliding performance of particulate-filled alloy composite. Maleque et al.[18] discussed that the digital logic method and unit cost method are used for analysis of material performance. Similar results are reported by Maniya[19] which suggested that the material selection and ranking preference order are determined by using presence selection index method. This method is useful for design engineers to select the material for specific applications. Thus, the current study work attempts to—

(i) Design and development of ZA-27-Gr alloy composites fabricated by using high vacuum stir casting process.
(ii) Evaluation of physical, mechanical, and sliding wear performance of ZA-27 -Gr alloy composite.
(iii) Investigate the L_{16} orthogonal array of the Taguchi approach that is used to optimize the wear parameters for ZA-27-Gr composites.
(iv) ZA-27-Gr alloy composite ranking material performance analysis utilizing the PSI method.

Materials and Methodology

Materials, Design and Fabrication Procedure

Rods made of the ZA-27 alloy were purchased from Bharat Aerospace Metals in Mumbai, India, having aluminum (25–28 wt%), copper (1.0–2.5 wt%), magnesium (0.01–0.02 wt%), iron (~0.075 wt%), lead (~0.006 wt%), tin (~0.003 wt%), and zinc rest wt%, while graphite particulates (99 μm) were procured from Savita Scientific Pvt. Ltd. Jaipur. Four alloy composites (AGr-0, AGr-2, AGr-4, and AGr-6) with different quantities of graphite (0, 2, 4, and 6 wt%) were produced using a high vacuum casting technique. The chemical composite composition is AGr-0 (0 wt% Gr; constant 2 wt% of Mg constant; rest ZA-27 alloy), AGr-2 (2 wt% of Gr; constant 2 wt% of Mg; rest ZA-27 alloy), AGr-2 (2 wt% of Gr; constant 2 wt% of Mg; rest ZA-27 alloy), AGr-4 (4 wt% of Gr; constant 2 wt% of Mg; rest ZA-27 alloy), AGr-6 (6 wt%Gr; constant 2 wt% of Mg; rest ZA-27 alloy),

The precise fabrication process is as follows:

(i) The specified quantity of long ZA-27 alloy rods was cleaned, and their cut-up parts were then melted in a graphite crucible using a high vacuum induction furnace. The temperature dropped to a range between 660 °C and 430 °C when the melt quantity was kept at 870 °C for 20 minutes (the solidus and liquid temperature of the alloy).
(ii) The quantity of reinforcements was individually warmed at 300 C for 3 hours.
(iii) 2 wt% of magnesium powder was added to the molten metal to increase the wettability of the gr phase.
(iv) A fully automatic magnetic stirrer (stainless steel; 280 rpm; 10 min.) was used to achieve uniform addition of graphite phase in the molten melt.
(v) The mixture was put into an immovable 150 x 90 x 10 mm^3 cast iron mold and permitted to solidify to 30 °C in air for at least 45 minutes.
(vi) The specimens were cut using a wire electric discharge machine (EDM) in accordance with ASTM B387 standards, and the measurements were polished with sandpaper of various grit sizes

Physical and Mechanical Characterization

The physical characteristics of the ZA-27- Gr-reinforced alloy composite include its actual density, theoretical density, and void fraction. The actual/experimental density of the design composite specimen/water displacement method was used to calculate the void fraction. The Archimedes principal approach was used to calculate the experimental density of planned composite specimens in

accordance with ASTMD792 standard. With the aid of Eqn. 1,[20] the theoretical density of the specimens was calculated using the law of mixture:

$$\rho_c = \frac{1}{(\frac{W_p}{\rho_p}) + (\frac{W_m}{\rho_m})} \quad \text{Eqn. 1}$$

where W represents to weight fraction, ρ represents to density of the particulates and matrix phases, respectively. The voids fraction of designed composite samples is measured using Eqn. 2.[17]

$$\text{Voidfraction} = \frac{\text{Theoretical}(\rho t) - \text{Experimental}(\rho e)}{\text{Theoretical}(\rho t)} \quad \text{Eqn. 2}$$

The design composite specimen's hardness was calculated using the micro-Vickers hardness tester (Walter Uhltesting tester; ASTM E92 standard). For the hardness test, specimens were subjected to a 190 g weight for 10 seconds. Each specimen's indentation is carried out using a hardness-grade diamond indenter. Each design composite specimen underwent five different hardness tests at different sites, and the average of those results is calculated using Eqn. 3:

$$\text{HV} = 1.854\frac{\text{L}}{\text{D}} \quad \text{Eqn. 3}$$

where L is the applied load (g and D is the diagonal diameter (mm) of indenter).

On the UTM apparatus (ASTM: E-8) and using parameters such as the specimen's (flat shape) dimension of 160 × 10 × 10 mm^3, span length of 75 mm, and cross-head speed of 2 mm/s, a tensile test of a developed composite specimen was conducted. A universal testing device (ASTM: E-290) was used to conduct a flexural experiment on developed composite samples under real-world conditions. The chosen parameters were as per the ASTM E- 290 standard: specimen dimension = 50 × 10 × 10 mm^3, span length = 40 mm, and cross-head speed = 2 m/s. Using the equation, the flexural strength (F) is calculated. 4:[12]

$$\text{F} = \frac{3\text{PL}}{2\text{bt}^2} \quad \text{Eqn. 4}$$

where P = load (kg); b = width of specimen (mm); t = sample thickness of sample (mm); L= span length of the sample (mm).

The compression strength of the composite specimen was measured using the compression test (ASTM E9-09) and taken parameter as (specimen size = 10 ×10 × 10 mm^3; span length = 0.5 mm; speed = 2 m/s) and compression test was performed on UTM. The design of the composite specimen (impact strength) was conducted on impact tester equipment (as per ASTME-23) and selected the machine parameter as (specimen size = 64 × 12.8 × 3.2 mm^3; depth of notch =10.2 mm.[21]

Sliding Wear Tribo-Meter

Friction and tribological performance were assessed using the Multi-Specimen Tribo-tester (Model: TR-705; Ducom; ASTM G-99) (Figure 1). The machine specifications are rotating disk = 62 HRC hardened steels; specimen dimension = 14× 9× 10 mm^3 and load applied on fixed specimen in vertical direction. The factors that made up the condition of steady-state wear performances were constant load of 20 N and sliding velocity of 1, 1.25, 1.5, and 1.75 m/s. On the tribo-tester, sliding behavior study (five repetitions, 700 m each; constant disk track diameter = 40 mm) was carried out in order to determine the composite wear rate. All test result data were performed at environmental condition. The abrasive paper was used to clean the disk gently along with acetone after each trial, so that any kind of deposited on the disk may be cleaned out, before the next experiment trial. The sliding distance was one of the input operating parameters often used by research scholars wide across the literature. Hence, we have taken it as one of the input parameters. Lastly, each experimental data, the pin type sample was cleaned previously weighing by an EBM (Electronic Balance) machine (taken ± 1× 10^{-3} mg accuracy). From the machine, experimental data on wear rate and coefficient of friction were collected and analyzed. Therefore, the experimental specific wear rate data are shown in Table 2. The new developed alloy composite of specific wear rates (Ws) were obtained by following Eqn. 5.[22]

$$\text{Ws} = \frac{\Delta\text{m}}{\rho \times \text{vs} \times \text{t} \times \text{fn}} \quad \text{Eqn. 5}$$

where Δm = mass loss (g); density (ρ); the sliding velocity (vs); the test duration (t); the normal load (f_n).

Experimental Design and Surface Morphology Studies

An effective optimization method for various control elements, such as load, sliding velocity, filler content, and sliding distance, was the detailed Taguchi design approach, which also examined the sliding wear behavior of proposed composite materials. S/N ratio is used in this strategy to indicate performance attributes, and experimental data for the developed composite are gathered via (Eqn. 6). Therefore, the lower-the-better (LB) characteristics technique was used to examine the wear rate performance. The different input factors and their quantified values are listed in Table 1.

Wear rate is used as the output parameter in a Taguchi design of experiment (L16 orthogonal array). The lower-the-best characteristic of the S/N ratio is described in terms

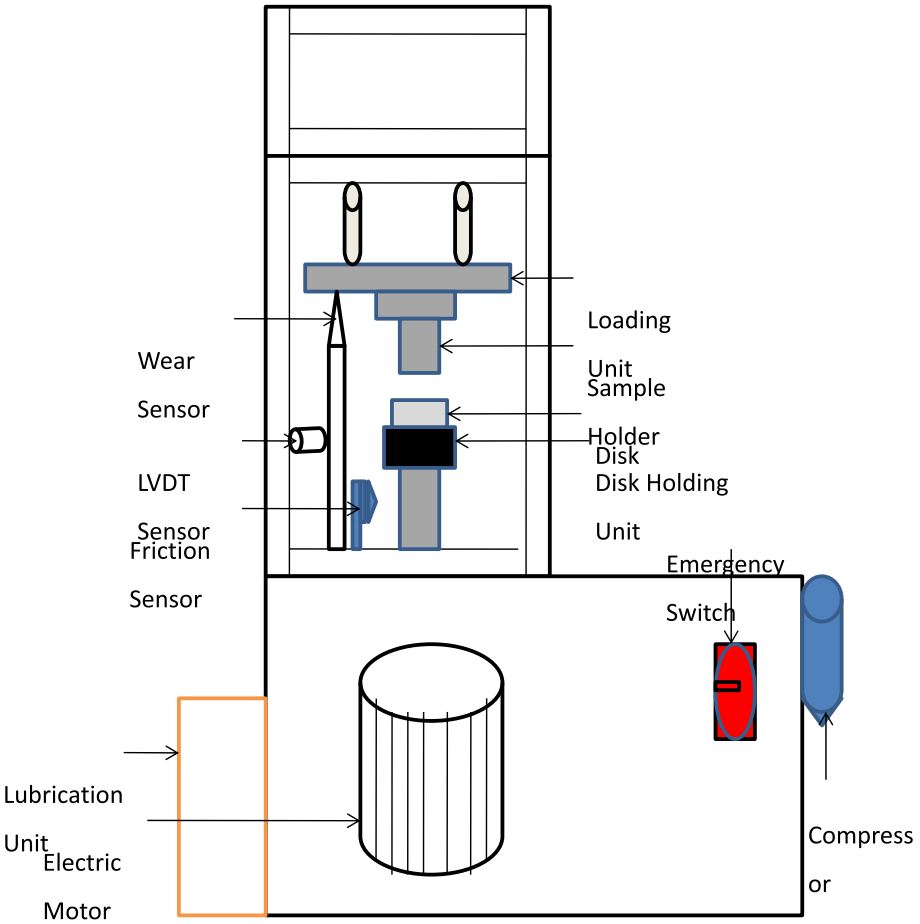

Figure 1. Hierarchy structure of the problem.

Table 1. Working Range of Selected Parameters

Control factor	Level				
	I	II	III	IV	Units
Normal load (*A*)	10	20	30	40	N
Filler content (*B*)	0	2	4	6	%
Sliding velocity (*C*)	1	1.25	1.50	1.75	m/s
Sliding distance (*D*)	700	1400	2100	2800	m

of Eqn. 6. Analysis of variance (ANOVA) is also used to rank the relevance of input parameters that have an impact on output performance (such as wear rate).

$$\frac{S}{N} = -10\log\frac{1}{N}\sum Y^2 \qquad \text{Eqn. 6}$$

where N= number of observation and Y= observed data.

In order to understand the wear process of developed composites, the field emission scanning electron microscope (FEI Nova Nano SEM 450, USA) is employed to examine the behavior of worn-out surfaces in SEM micrographs.

Preference Selection Index Method Algorithm

The PSI technique is a systematic scientific process or tool that design engineers can use to determine the optimal material for a certain application. This strategy is helpful when there is a disagreement over the relative importance of attributes, which is the PSI method's drawback. The following steps are a representation of the precise processes for PSI computation.[23–27]

Step 1: Structure of decision problem: For PSI to calculate for the specified application, data input is necessary to obtained all possible material alternatives and selection criteria. These methods aid in determining the objective. Numerous studies have claimed that the typical decision-making problem's hierarchy structure makes it easy to comprehend. The hierarchy should place the significant goal at the top, the ranking criteria in the center, and the

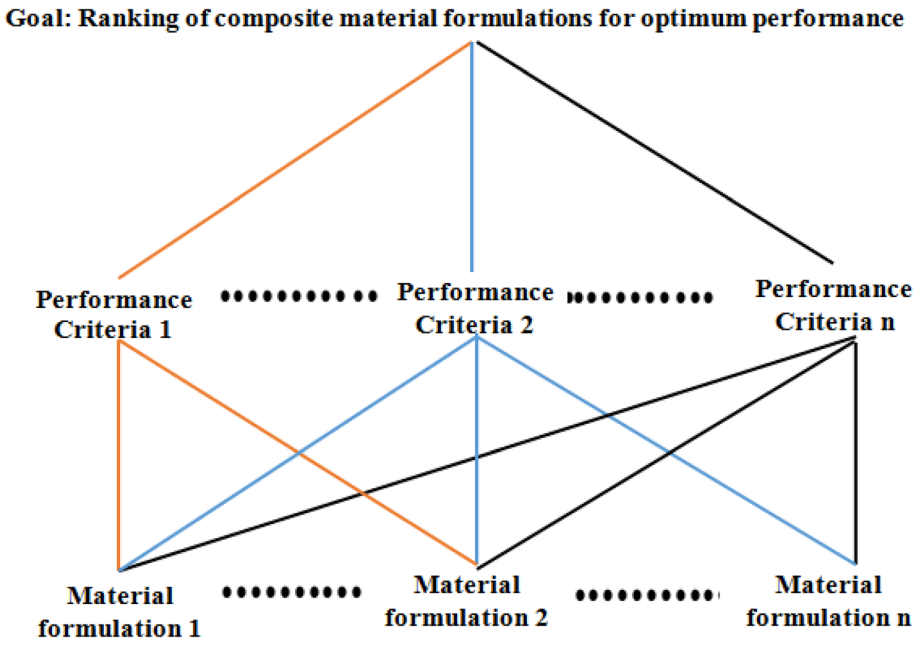

Figure 2. Effect of filler on density and voids content of developed composite.

alternatives/options at the bottom. As a result, Figure 2[28,29] shows the hierarchical structure of investigating problem.

Step 2: Formulate decision matrix: A multi-alternative (let's say, m-alternatives) and multi-criteria (let's say, n-criteria) problem is another way to represent the decision matrix product (say matrix D of $m \times n$ order).

$$D_{m\times n} = \begin{array}{c} \\ \mathrm{A}_1 \\ \mathrm{A}_2 \\ \vdots \\ \mathrm{A}_m \end{array} \begin{array}{c} \begin{array}{cccc} C_1 & C_2 & \cdots & C_n \end{array} \\ \begin{bmatrix} p_{11} & p_{12} & \cdots & p_{1n} \\ p_{21} & p_{22} & \cdots & p_{2n} \\ \vdots & \vdots & \ddots & \vdots \\ p_{m1} & p_{m2} & \cdots & p_{mn} \end{bmatrix} \end{array}$$

where C_1,C_2, ..., C_n are the n - criteria and

A_1,A_2, ..., A_m are the m - alternatives

The element p_{ij} is the performance value of the ith alternative (A_i) with respect to the jth attribute (C_j) where i =1, 2, …, m and j = 1, 2,…, n.

Step 3: Normalization of decision matrix: Normalization is a process of transforming the decisive data range of 0 to 1 and is needed in order to transform Performance rating with the various data measurement unit into a compatible unit. In order to compute all criteria in unit less and to facilitate inter-attribute comparisons; the entries of the above matrix are normalized (using below principle). Thus, find out normalized matrix is R_{ij}.

(i) If the expectancy is *larger-the-better*, then the original attribute performance can be normalized as follows:(Eqn. 7)

$$Rij = \frac{x_{ij}}{x_j^{max}} \qquad \text{Eqn. 7}$$

(ii) If the expectancy is *smaller-the-better*, then the original attribute performance can be normalized as follows:(Eqn. 8)

$$Rij = \frac{x_j^{min}}{x_{ij}} \qquad \text{Eqn. 8}$$

where x_{ij} is the attribute measures (i = 1,2,3, . . . , m and j = 1,2,3, . . . , n).

Step 4: Compute preference variation value (PV_j): The idea of sample variance analogue and the Eqn. 9, R_{ij} is used to measure preference variation value ($\mathrm{PV_j}$) for each criterion for determining normalized matrix.

$$\mathrm{PVj} = \sum_{i=1}^{N} \left(R_{ij} - \overline{R}_j\right)^2 \qquad \text{Eqn. 9}$$

where $\overline{R}_j$ is the mean of normalized value of criteria j, i.e., $\overline{R}_j = \frac{1}{n}\sum_{i=1}^{N} R_{ij}$

Step 5: Computation of overall preference value (ψ_j): The overall preference value (ψ_j) of every criterion is calculated using the following Eqn. 10:

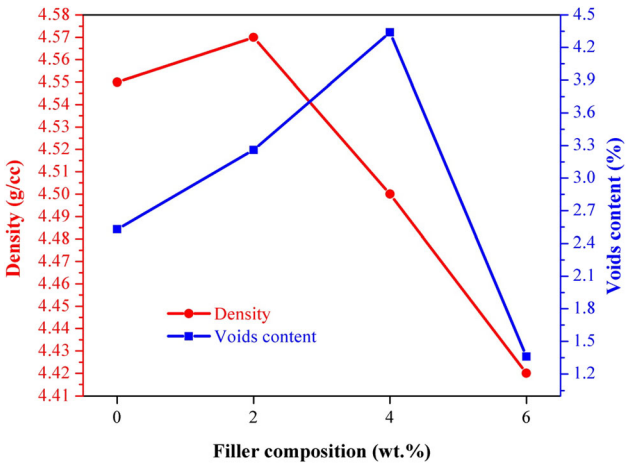

Figure 3. Multi-specimen tribo-meter (Model: TR-705 of Ducom Instruments).

$$\Psi j = \frac{\Phi_j}{\sum_{j=1}^{n} \Phi_j} \qquad \text{Eqn. 10}$$

where $\Phi_j = 1 - \Sigma PV_j$ is the deviation in the preference value of each criteria. For consistency, the sum of overall preference value for all the criteria should be unity, i.e., $\Sigma \psi_j = 1$.

Step 6: Computation of Preference Selection Index (I_i): The preference selection index (I_i) for each alternative is measured using the following Eqn. 11:

$$I_i = \sum_{j=1}^{n} (R_{ij} \times \Psi_j) \qquad \text{Eqn. 11}$$

Step 7: The computed values of preference selection index (I_i): The computed values of preference selection index (I_i) are used to rank the alternatives according to its descending order, i.e., highest to lowest I_i value is used to rank the alternatives from first to last and then making related interpretations or recommendation.

Results and Discussion

Physical and Mechanical Characteristics

Effect of Filler on Voids Content/Density of Developed Composite

Figure 3 illustrates the effect of graphite on void content of varying wt% filler (0, 2, 4 and 6 wt%)-filled zinc–aluminum (ZA-27) alloy composite. The experimental outcomes of the void fraction of designing composites are obtained from the both densities as (theoretical/experimental). Void fraction of designing alloy composites is slowly improving by an increment in reinforcement, while

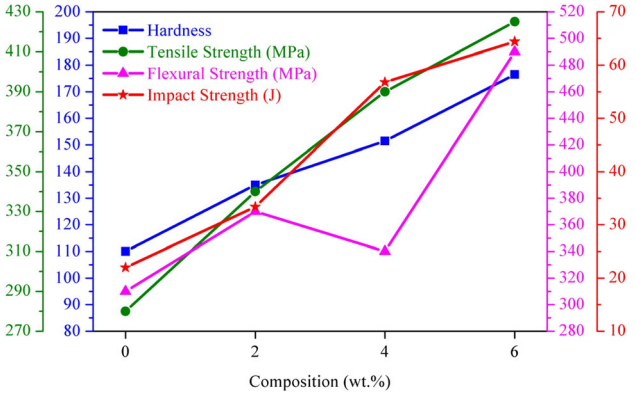

Figure 4. Effect of filler on mechanical characteristics of developed composite.

the void fraction of 6 wt% Gr-ZA-27 alloy composite shows the decreasing trend. This may be attributed that the equal presence of particulate increases the interfacial bonding between base matrix and reinforcement, therefore, minimize the voids present in alloy composite. It may decrease the void content by providing the movement and arrangement facilities to the reinforcements since clustering will take place by mixing larger number of reinforcements in matrix materials.[54,55] The higher weight percentage of void contents shows minimum due to the proper mixing of reinforcement and matrix of composite. It may be that the void fraction shows the negative impact in strength of materials and wear rate of composite. Hence, the void content decreases with increase in hardness of composite.

The variation in density with increase in graphite powder-filled ZA-27 alloy composite is employed in Figure 3. It is observed that the density of designing composite decreases with enhancement in graphite content. The density of the neat alloy composite is 4.55g/cc and addition of 2 wt% Gr-reinforced ZA-27 alloy composite of density is 4.42 g/cc (7.2% reduction). Further addition of 4 wt% Gr powder of density is 4.30 g/cc (4.4% reduction). Again, addition of 6 wt% Gr powder of density is 4.36 g/cc (3.6% reduction) against the base alloy. It can be noted that the density of composite decreases due to the lower weight of Gr particle compared to the base alloy. The density of composite decreases with increase in particulate of rice/Sic powder.[12,30]

Effect of Graphite on Hardness of Alloy Composite

Figure 4 depicts the effect of graphite on the hardness of designed alloy composites. It is observed that the hardness of designed alloy of composite is increased with increment in reinforcement. The ZA27-6 wt% Gr alloy composite shows the higher hardness compared to neat alloy composite. It is observed from the graph; the neat alloy composite of hardness shows 107 HV. Further, addition of 2

wt% graphite powder-filled alloy composite shows increase in hardness (135 HV). Again, increment of 4 wt% and 6 wt% graphite powder-filled neat alloy composite shows increase in hardness 157 HV and 171 HV. Similar results are reported by Abdizadeh et al.[31] that the hardness of the said composites may increase because of increase in the content of graphite particulates reinforcing phases into the matrix. Sharma et al.[32] reported that enhancement in addition of graphite-reinforced particle increases the hardness of composite due to bonding strength and load carrying capacity of matrix to reinforcement increase. Rajmohan et al.[33] revealed that mixed of the mica increased the hardness of composite, thereby improving the machinability of fabricated composite.

Effect of Graphite on Flexural Strength of Alloy Composite

Figure 4 shows the variation in flexural strength on graphite-filled ZA-27 alloy composite. It is observed that the flexural strength of the designed specimen increased with increment in graphite reinforcement. The flexural strength of designed composite is higher at 0 wt% graphite content. Addition of 2 wt% Gr content of the flexural strength is decreased. Further addition of 4 wt% and 6 wt% graphite content of the flexural strength graph is showing continually increasing trend. Therefore, this may be that the proper distribution of particle and strongest bonding due to proper casting process. The flexural strength of designed specimen increases with the enhancement in the graphite content. It may be the flexural strength increase due to increase in ductility with lower material deformation. It seems that the interfacial bonding between the matrix and reinforcement is very strong. The outcomes are in excellent agreement with other investigation in this area.[34]

Effect of Graphite on Tensile Strength of Alloy Composite

Influence of graphite particles on tensile strength of zinc–aluminum (ZA-27) alloy composite is depicted in Figure 4. Tensile strength of designed composite was calculated by utilizing the software-based computerized UTM Machine. It was observed that the tensile strength outcomes improve with enhancement in graphite content. The designed specimens of tensile strength increase owing to enhance in hardness and strength of composite and addition of graphite causes the designed specimen of tensile strength increments with diminished in the percentage of elongation.[35] It is observed that the designed specimen of tensile strength is 290 MPa at 0 wt% Gr reinforcement. Further addition of 2 wt% Gr content of designed specimen of tensile strength is 340 MPa. Again, addition of 4 wt% Gr and 6 wt% Gr content of composite strength is 395 and 428 MPa. Similar observations are made by Ramnath et al.[36] It seems that the composites exhibit strong interfacial bonding between matrix and reinforcement along axial direction (tensile loading direction). It may be that the most

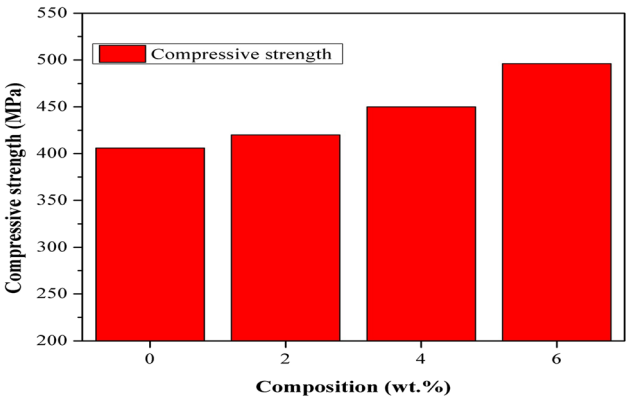

Figure 5. Effect of filler on compressive strength of developed composite.

grounded holding among base material matrix and filler are playing a significant contribution in improving the specimen strength of composite.

Effect of Graphite on Impact Strength of Alloy Composite

The effect of graphite particles on impact strength of ZA-27 alloy composite is employed in Figure 4. It is noticed that the impact strength of composite increases with increment in weight percentage of Gr. The designed composite specimen of impact strength is 23.56 J at 0 wt% Gr content. Again, expansion of 2 wt%, 4 wt% and 6 wt% of the reinforced content of impact strength of composite is 33.5 J, 58.5 J and 64. J. The 6 wt% graphite-reinforced-based composite of impact strength is higher compared to other compositions. It may be attributed to alloy composite's presence in minimum voids, while it was higher impact strength for composite. Same findings are stated by Ozden et al.[37] that manifested the impact strength increased owing to improved resistance ability. The impact strength of composite slightly enhances with increase in the particle size and hot extrusion ratio also enhanced impact strength due to the influence of temperature.[31] Therefore, impact strength of composite increases with the addition of Gr content owing to ductile fracture in the material, excellent holding reinforcement in the matrix, and cracking in the material deposited at the energy of plastic deformation. The increased impact strength gives the created composites remarkable resistance capabilities. As a result, it seems that the reinforcing phase successfully arrested cracking failure of composites to a great extent, owing to enhanced interfacial bonding.[54]

Effect of Graphite on Compressive Strength of Alloy Composite

The effect of compressive strength on graphite powder-filled ZA-27 alloy composite is employed in Figure 5. The compressive strength of designed specimen increases with

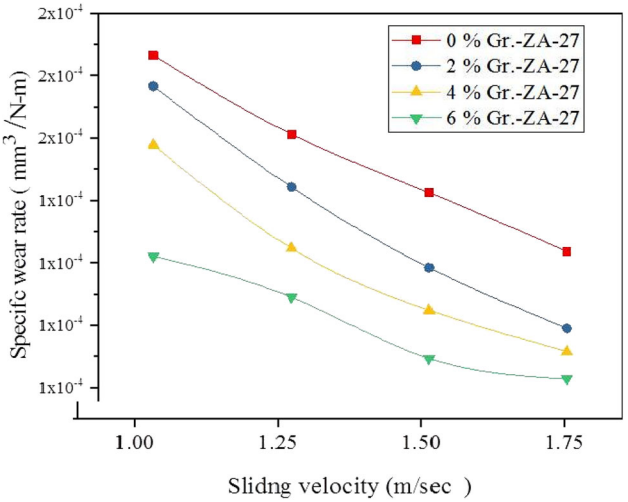

Figure 6. Effect of sliding velocity on specific wear rate.

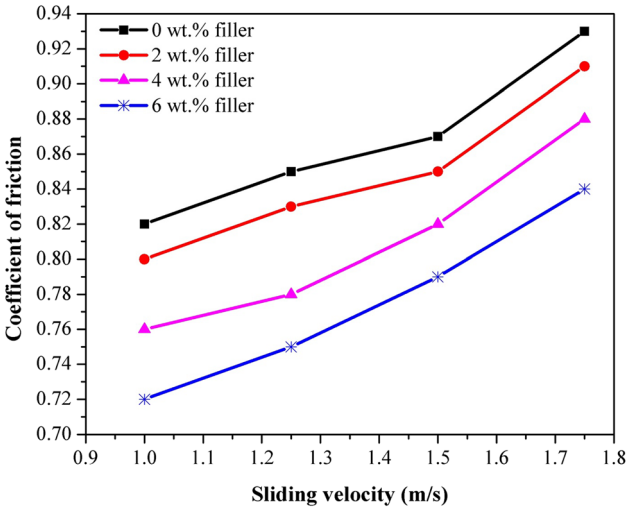

Figure 7. Effect of sliding velocity on coefficient of friction.

the increasing graphite content. It is seen from the graph that the compressive strength of designed composite is higher as comparatively unfilled alloy. The higher strength value of designed composite is 496 MPa at 6 wt% Gr content and without addition of graphite of strength value is 406 MPa at 0 wt% Gr content. Further addition of 2 wt% and 4 wt% Gr content of strength is 420 MPa and 450 MPa.

The 6 wt% graphite-reinforced-based alloy composite of compressive strength is maximum, while the compressive strength of other compositions is slowly gradually improving with increment in Gr content. The compressive strength increases with Gr addition due to the better interfacial bonding and hard nature of reinforcement particles with matrix material which resist the deformation of material during the mechanical characterization.[54] The improvement of compressive strength may be owing to the addition of different reinforcements like SiC, B4C, Gr, and Cu powder that were reported by another researcher/scientist. Therefore, the compressive strength of composite increases due to graphite particulates, dislocation, and strength mechanism.[55]

Wear Experimental Studies

Effect of Sliding Velocity on Specific Wear Rate and Coefficient of Friction

The influence of sliding velocity on specific wear rate of ZA-27 –Gr-reinforced alloy composites is employed in Figure 6. Wear steady-state wear experiment of ZA-27-Gr-reinforced alloy composites is conducted on four distinct sliding velocities like (1, 1.25,1.50 and 1.75 m/s) and other two variables are taken as constant normal load (10 N) and sliding distance of 700 m. The designed composite of wear rate reduces with the enhancement of the graphite content and it is found to be lower at 6 wt% Gr content as compared to another designed composite. It is found that the composite of wear rate is higher for 0 wt% as compared to other compositions. The decrease in wear rate owns to the addition of graphite reinforcement which works as a solid lubricant and it forms a skinny layer among the mating surface. Reduction in wear rate is due to the increase in sliding velocity. Wear behavior was observed with the trends reported by few researchers/materialist.[38,39] It is observed that the presence of graphite particulates minimizes the voids content, crack propensity, and form tribo-layer over the surface. This minimizes the abrasion and hence the wear rates.[8]

The influence of sliding velocity on coefficient of friction of Gr-reinforced zinc–aluminum alloy composites is employed in Figure 7. This decrease in coefficient of friction is due to the addition of graphite content and the COF value improves with increase in sliding velocity. It was found that the 0 wt% Gr-reinforced zinc–aluminum alloy composite exhibits the higher value of (μ) which was 0.93 at 1.78 m/s of sliding velocity as compared to designed wt% of composite. It may be that the increment in sliding velocity of the composite increases with COF. It is obtained from the graph that the μ (coefficient–of- friction) of 6 wt% Gr-ZA-27 developed composite shows lower relative to specific designed composite. This might be attributed that the coefficient of friction (COF) enhanced due to the non-breakable asperities action on cutting tool, that can be destroyed surface of the material on scratches or deep grooves in the incidence of non -breakable asperities from the exhausted surface of alloy composite. The other reason is that the deformation of material between the flat specimen and spinning disk can be partially accounted for the grater of coefficient of friction. The higher loss of

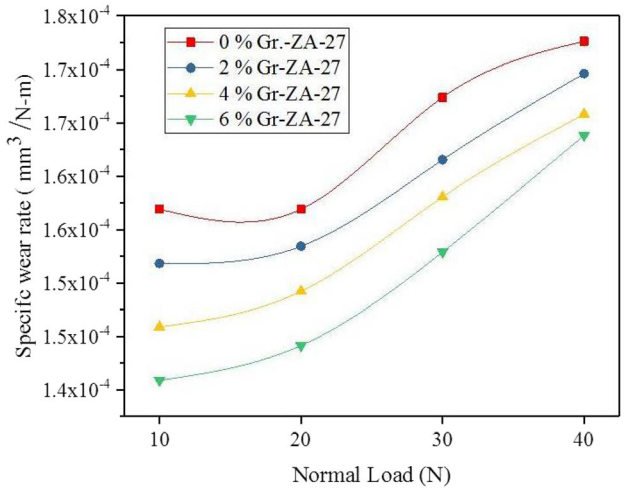

Figure 8. Effect of normal load on specific wear rate.

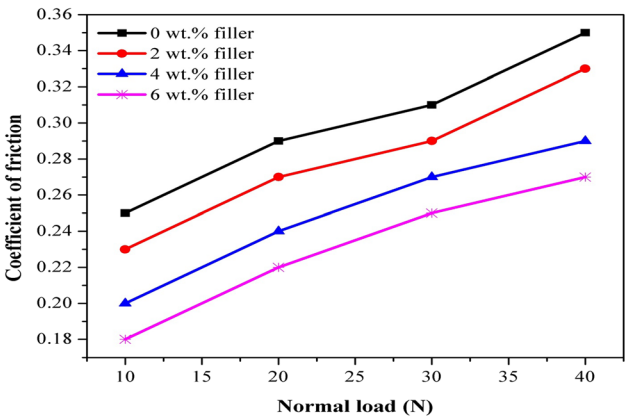

Figure 9. Effect on normal load on coefficient of friction.

material is generated at a maximum sliding velocity and high friction of materials.[12,40]

Effect of Normal Load on Specific Wear Rate and Coefficient of Friction

The influence of normal load on specific wear rate of ZA-27 –Gr-reinforced alloy composites is depicted in Figure 8. Wear steady-state wear experiment of ZA-27-Gr-reinforced alloy composites is conducted on four distinct normal load like (10, 20, 30 and 40 N), and other two variables are taken as constant sliding velocity (1 m/s) and sliding distance of 700 m. It was observed that the wear rate of designed Gr –ZA-27 alloy composites increases with increase in applied load and wear rate of composite increases with addition of graphite also. This may be that the wear rate increases due to addition of reinforcement. In sliding test condition, the graphite is used as solid lubricant and it produces a skinny layer graphite coating in the upper section of the counter surfaces, which stops sub-surface contact through sliding. Hence, as load increases, the composite's wear rate (W) increases. The wear rate order is 0 wt% GR-ZA27 > 2 wt% GR-ZA27 >4 wt% GR-ZA27 > 6 wt% GR-ZA27. The good wear performance of 6 wt% GR-ZA27 alloy composite might attribute to the zinc–aluminum matrix and graphite content shows good adhesion bonding condition between matrix and filler content. The fabricate composite of hardness reduces due to the higher porosity which shows increase in the wear rate of composite with increase in the normal load. Similar results are reported by different scientist/researchers.[41,42]

The influence of variation in normal load (10–40 N) on COF(μ) of Gr-filled zinc–aluminum composites is shown in Figure 9. It is evident that the (COF) value increases with an increase in the normal load; which shows the trend of COFvalue remains constant 10–20 N applied load at the various wt% of filler content. After some time, the load (30–40 N) value enhanced; then, the COF increased from 0.28 to .31 for 0 wt% of Gr-filled ZA-27 alloy composite which shows that this designed alloy composite of COF has the best results compared to other investigated alloy composites. Designed alloy composite of COF order is as follows: 0 wt% Gr–ZA-27 > 2 wt% Gr-ZA-27 > 4 wt% Gr-ZA-27 > 6 wt% Gr-ZA-27. This may be the (COF) value increases with increment in load because of the development of mechanical layer and fragmentation of asperities debris particles during the sliding condition. It is observed that for 6 wt% Gr-filled zinc–aluminum (ZA-27) alloy, composites depict the lower friction with increasing applied load due to various mechanisms of wear and thermal softening below the exhausted surface as an outcome of enhanced the temperature.[4] It is observed that this designed composite leads to the reducing of the coefficient of friction in the composite and decreases the pin to disk contact. Hence, it can be concluded that the addition of the graphite content to unfilled alloy improves the wear behavior, performance of the designed composites, far better than that of the matrix alloy, and the wear and coefficient of friction reduce with increasing the graphite content.[34]

Effect of Sliding Distance on Specific Wear Rate and Coefficient of Friction

The influence of sliding distance on specific wear rate of ZA-27 –Gr-reinforced alloy composites is depicted in Figure 10. Wear steady-state wear experiment of ZA-27-Gr-reinforced alloy composites are conducted on four distinct sliding distances like (700, 1400, 2100 and 2800 m) and other two variables are taken as constant sliding velocity (1 m/s) and normal load of 700 m. The effect of the wear rate on changing the sliding distance of Gr-reinforced ZA-27 alloy composite is depicted in Figure 10. It is observed that the designed composites of wear rate increase with an increase in distance of sliding of composites. The wear rate order is followed as 0 wt% Gr-ZA-27

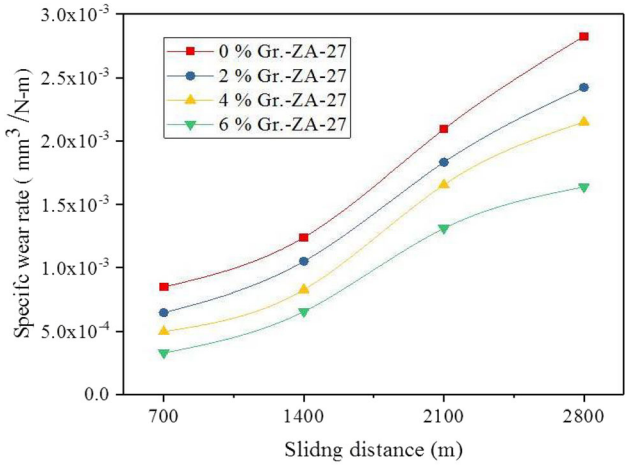

Figure 10. Effect of sliding distance on specific wear rate.

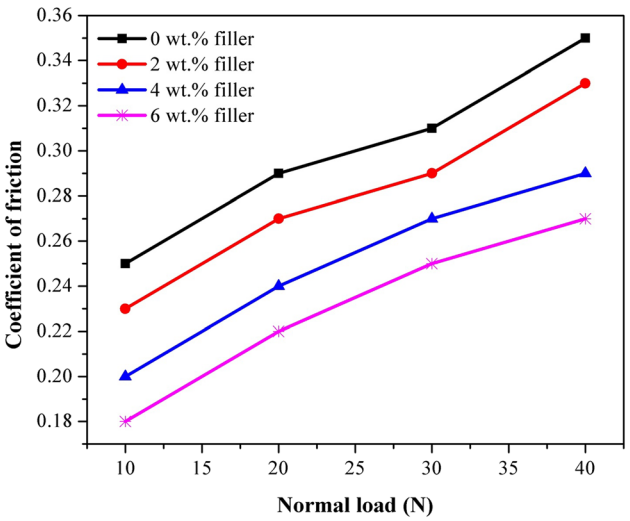

Figure 11. Effect of sliding distance on coefficient of friction.

> 2 wt% Gr-ZA-27 > 4 wt% Gr-ZA-27 > 6 wt% Gr-ZA-27. It was clearly seen from the graph that the wear rate of composite depicts the lower value at a lower sliding distance (700 m), but beyond the increased 1400 to 2800 m sliding distance of specific wear was enhanced. In general, base alloy composites have a higher wear rate than other composites, despite having a larger weight proportion of alloy. The reason that the wear rate of designed composites is improved with an increment in the sliding distance because of the bottom section of sliding disk is stable, then the particles are fractured and exhausted debris particles occur through the counter surface. It may be that surface contact area of sliding is increased with increase in interaction time and rotation of disk, then enhanced the specific wear rate.[37]

The influence of varying sliding distance (700–2800 m) on COF (μ) of Gr-filled zinc–aluminum (ZA -27) alloy composites is depicted in Figure 11. The value of COF (μ) increases with increment in Gr (0–6 wt%) content of alloy composite. The designed composite of COF value shows the higher at 0 wt% graphite content and lower value of COF shows at 2wt% Gr powder-reinforced ZA -27 alloy composite. The decreasing wear rate trend suggests that the reinforcing particulate shape, size, content, and distribution have an impact on the wear rate of the alloy composites. It is observed that the magnitude of COF was lower at a lower sliding distance for alloy composite. The COF of composite slowly improves with increment in sliding velocity for Gr-filled zinc–aluminum alloy composite. It may be the COF(μ) improved with increment in sliding distance due to the grain growth; hardness increases in wear resistance.[12,43]

Analysis of Experimental Results by Taguchi Experimental Design and ANOVA Method

The Taguchi method is used as an estimation tool for calculating robustness and the signal-to-noise (S/N) ratio is the very valuable component of a parametric design. In this method, the word 'signal' indicates the desirable goal, i.e., wear rate and the word 'noise' indicates the undesirable value. The S/N ratio data listed in Table 2 are in details the average of two replications. The entire mean for the S/N ratios of designed composites filled with graphite content is observed as 75.25 dB, respectively. The Taguchi data are analyzed via MINITAB 14 software. First, any test is made to utilize this model as a forecast for the estimate of performance, and the suitable interactions between the control parameters must be considered. However, the interaction effect is measured through factorial design of composite. The influences of control factors on wear rate are indicated in Figure 12, respectively. An entire sequence of significance of control parameters in diminishing rate of composite, i.e.; (normal load (L) > reinforcement (R) > sliding velocity (V) > sliding distance (SD).[44,45]

ANOVA was utilized to observe the % (percentage) share of control factors in calculating retort, i.e., wear rate of composite. The investigations conducted on 5 % (level of significance). The obtained order by ANOVA is, i.e., normal load (41.81%) > reinforcement (22.98%) > sliding velocity (14.55%) >Sliding distance (11.53) (Table 3). The sequence of significant control factor confirms that controls the entire mechanism of wear system.

The last step of Taguchi methodology was to perform confirmation tests in order to validate the conclusion made in the above analysis phase. For this, an arbitrary factor

Table 2. Experimental Response Table for L16 Orthogonal Array Layout

S.No.	Normal load	Filler content	Sliding distance	Sliding velocity	Specific wear rate(mm^3/N-m)	S/N ratio (dB)
1	10	0	700	1	0.000188300	74.5030
2	10	2	1400	1.25	0.000193836	74.2513
3	10	4	2100	1.5	0.000265287	71.5257
4	10	6	2800	1.75	0.000163827	75.7123
5	20	0	1400	1.5	0.000337371	69.4378
6	20	2	700	1.75	0.000371519	68.6004
7	20	4	2800	1	0.000360625	68.8589
8	20	6	2100	1.25	0.000196592	74.1287
9	30	0	2100	1.75	0.000118559	78.5213
10	30	2	2800	1.5	0.000191144	74.3728
11	30	4	700	1.25	6.63218E-05	83.5669
12	30	6	1400	1	8.19135E-05	81.7329
13	40	0	2800	1.25	0.000125534	78.0248
14	40	2	2100	1	0.000115763	78.7286
15	40	4	1400	1.75	0.000116063	78.7061
16	40	6	700	1.5	0.00018021	74.8844

Table 3. Wear Rate of Response of ANOVA Table for S/N Ratios

Source	DF	Seq SS	Adj SS	Adj MS	*F*	*P*	*P* (%)
Normal load (*L*)	4	1300.72	1226.63	340.46	7.87	.019	41.81
Filler content (*F*)	4	651.06	648.73	120.86	5.08	.188	22.98
Sliding velocity (*V*)	4	641.13	685.85	187.52	6.67	.115	14.55
Sliding distance (*D*)	4	2472.72	1462.89	362.48	8.19	.016	11.53
Error	8	504.33	534.35	64.47			9.15
Total	24	5569.96					100

S = 8.24402 *R*-Sq =90.54% *R*-Sq (adj) =80.93% *DF* degrees of freedom, *Seq SS* sequential sums of squares, Adj *SS* adjusted sums of squares, Adj *MS* adjusted mean squares, *F* variance, *P* probability.

combination says $A_4\ B_2\ C_5\ D_4\ E_1$ would be taken to predict the SWR. The predictive Eqn. 5 may be used to estimate the S/N ratio for the SWR

$$\overline{\eta_1} = \overline{T} + \left[\overline{A_4} - \overline{T}\right] + \left[\overline{B_2} - \overline{T}\right] + \left[\overline{C_5} - \overline{T}\right] + \left[\overline{D_4} - \overline{T}\right] + \left[\overline{E_1} - \overline{T}\right] \quad \text{Eqn. 12}$$

where $\overline{\eta_1}$ is the predicted average; $\overline{T}$ is the overall experimental average; $\overline{A_4}, \overline{B_2}, \overline{C_5}, \overline{D_4}$ and $\overline{E_1}$ are the average response for the factors at respective levels. The S/N was found to be $\overline{\eta_1}$ = 78.29 dB using Eqn. 5. After that, conformational test trials were performed for the factor combinations ($A_4\ B_2\ C_5\ D_4\ E_1$) settings. The obtained results 75.25 dB were then compared with the predictive result ($\overline{\eta_1}$) (Table 4) and an error of 3.88% has been found. The computed error may further be reduced by more experimental trials. Thus, the model suitably predicts the SWR of the alloy composites with reasonable accuracy.

Surface Morphology of Alloy Composite

The SEM micrograph of graphite-reinforced with zinc–aluminum (ZA-27) alloy composites for steady-state wear experiment condition like (Taguchi DOE; L16 orthogonal array) at varying load (10–40 N) is presented in Figure 13a–d. It was evident that from an SEM micrograph Figure 13a; the wear rate (WR) of unfilled alloy composites was (0.0001883 mm^3Nm^{-1} at level 1; Table 2). In the SEM micrograph of ZA-27/0 wt% Gr (Figure 13a), delamination is observed due to a lower load, i.e., 10 N and lower sliding velocity 1 m/sec velocity. The delamination may be generated due to less frictional heating between the counter face and large amount of material is removed on sample surface and delamination occurs at lower load and sliding velocity.[44] In Figure 13b, 2% Gr-filled ZA-27 alloy composite demonstrates the specific wear rate, i.e., 0.000371519 mm^3Nm^{-1} (Exp. Run 6, Table 2) with (steady-state parameter like sliding distance =700 m;

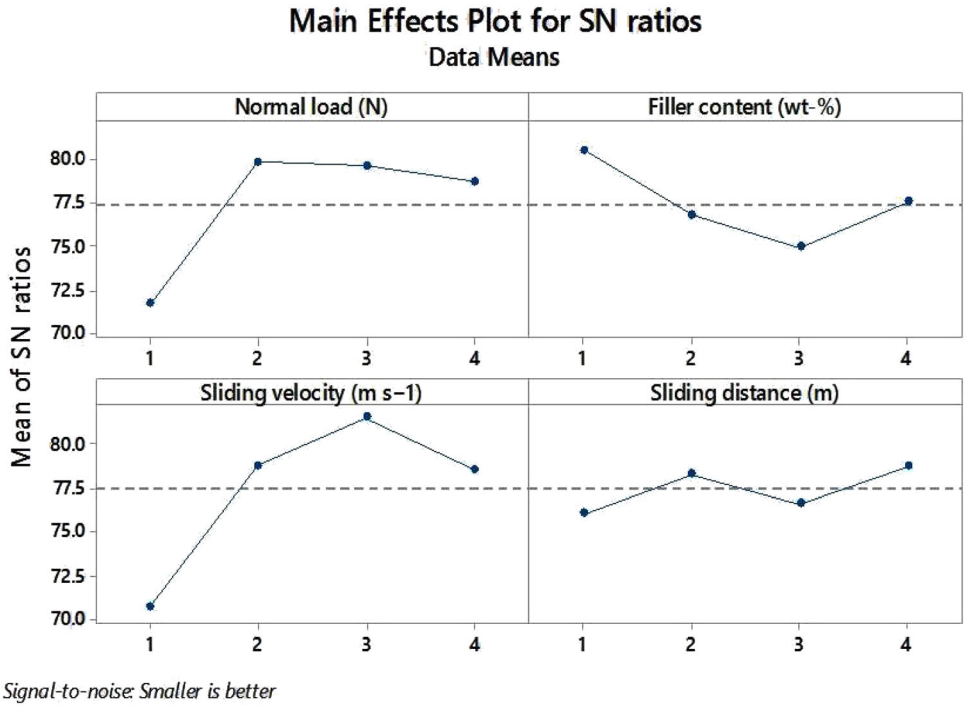

Figure 12. Influences of control factors on specific wear rate.

Table 4. Results of the Confirmation Experiment for SWR

	Optimal control parameter		
	Prediction	Experimental	Error
Level	A_4 B_2 C_5 D_4 E_1	A_4 B_2 C_5 D_4 E_1	
S/N ratio for SWR (dB)	78.29	75.25	3.88 %

normal load= 20 N; and sliding speed = 1.75 m/ s). In steady-state sliding tests, when the two flat pieces are rubbed together, it generates friction heats at the interface of material surface because of the mellowing of surface; impairment of wear particles and shallow Groves of composite.[46]

Figure 13c shows the specific wear rate for the 4 wt% Gr filled ZA-27 alloy composite. 0000663218 mm_3Nm-_1 (exp. run 11, Table 2) with steady state parameters such as sliding distance = 700 m, normal load = 30 N, and sliding speed = 1.25 m/s. The particle of debris (PD) is seen on the exhausted surface underneath the utilization of increment of load. (The interface heat is created due to the mellowing of the surface and impairment of wear particles.)[47] The SEM micrograph of sliding wear Figure 13d of 6 wt% of Gr-filled ZA-27 alloy composite indicates the wear rate (SWR) is 0. 0.00018021 mm^3 Nm^{-1} (exp. run 16; Table 2) at steady state of sliding wear parameter like ("High sliding velocity =1.5 ms^{-1}; Normal Load =40 N; sliding distance =700 m"). The plowing mechanism generates because of maximum content of plastic deformation. The similar finding is reported by various researchers.[48–53]

Ranking Optimization Using PSI Method

In this research chapter, PSI method is applied on the decision matrix (D), having performance criteria shown in Table 5, with four composite specimens as alternatives (namely, AGR0, AGR2, AGR4 and AGR6). The step-wise computations are as follows:

Step 1: The evaluated performance data are organized in the form of decision matrix shown in Table 6.
Step 2: Table 7 shows normalization of the decision matrix as per the algorithm.
Step 3-7: Table 8 shows the intermediate calculations and the final ranking order of alloy composites obtained as per the algorithm.

Conclusions

ZA-27–GR alloy composite was fabricated by the high vacuum casting method. The mechanical and tribological properties of ZA-27–GR alloy composites were analyzed by UTM machine and multi-specimen tester machine and

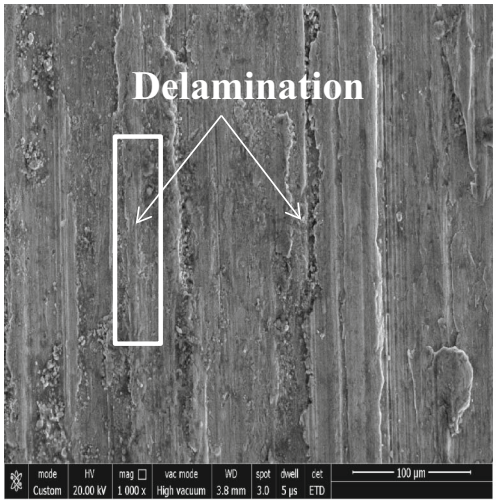

(a) AGr-0 at 10 N load

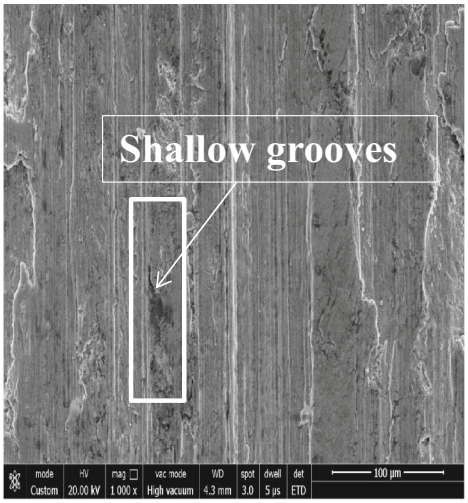

(b) AGr-2 at 20 N load

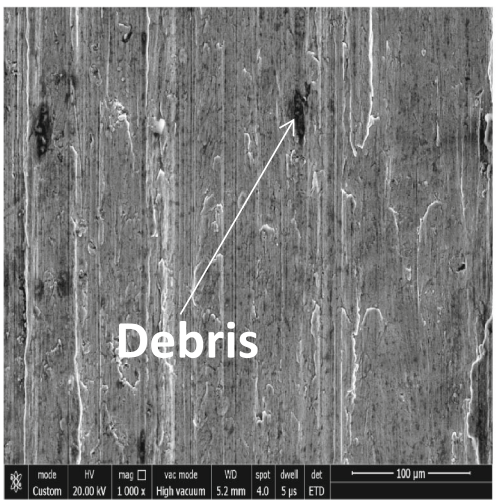

(c) AGr-4 at 30 N load

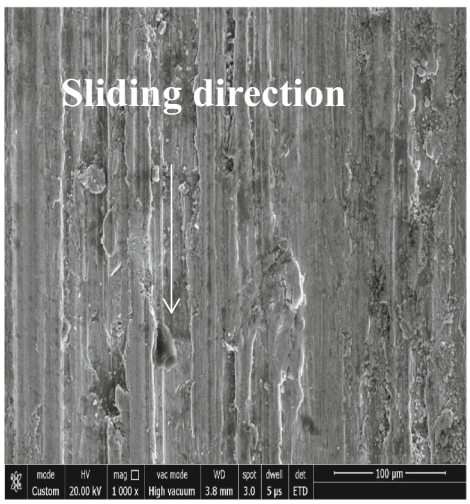

(d) AGr-6 at 40 N load

Figure 13. Wear surface micrograph.

Table 5. Descriptions of the Selection Criteria Applied in this Case Study

Sr. No.	Performance criteria	Preference
1	Tensile strength (MPa)	Maximum
2	Flexural strength (MPa)	Maximum
3	Impact strength (*J*)	Maximum
4	Hardness (HRB)	maximum
5	Compressive strength	maximum
6	Density (g/cc)	Minimum
7	Void content (%)	Minimum
8	Specific wear rate (mm^3/Nm)	Minimum
9	COF	Minimum

Table 6. Decision Matrix

PC's	Property	Material alternatives			
		0%	2%	4%	6%
PC-1	Tensile strength (MPa)	290	340	395	428
PC-2	Flexural strength (MPa)	300	363	342	490
PC-3	Impact strength (J)	22.76	33.5	58.5	64
PC-4	Hardness (HRB)	107	135	151	171
PC-5	Compression strength (Mpa)	406	420	450	496
PC-6	Experimental density (g/cc)	4.55	4.57	4.5	4.42
PC-7	Voids content (%)	2.53	3.26	4.36	1.36
PC-8	Specific wear rate at sliding distance (mm^3/Nm)	2.8	2.5	1.8	1.4
PC-9	Coefficient of friction at Sliding Distance	0.19	0.28	0.35	0.55

Table 7. Normalization of the Decision Matrix

PC's	Material alternatives				
	0%	2%	4%	6%	Mean
PC-1	0.67	0.78	0.91	1.00	0.84
PC-2	1.00	0.87	0.82	0.65	0.83
PC-3	1.00	0.91	0.78	0.62	0.82
PC-4	1.00	0.95	0.88	0.76	0.90
PC-5	0.82	0.85	0.91	1.00	0.89
PC-6	0.97	0.97	0.98	1.00	0.98
PC-7	0.54	0.42	0.31	1.00	0.57
PC-8	0.50	0.56	0.78	1.00	0.71
PC-9	1.00	0.68	0.54	0.35	0.64

Table 8. Ranking of the Composites

PC's	Material alternatives			
	0%	2%	4%	6%
PC-1	0.0906	0.1050	0.1159	0.0773
PC-2	0.1009	0.0946	0.0757	0.1161
PC-3	0.1030	0.0879	0.0697	0.1134
PC-4	0.1141	0.1055	0.0913	0.1198
PC-5	0.1028	0.1101	0.1214	0.994
PC-6	0.1196	0.1215	0.1237	0.1202
PC-7	0.0374	0.0280	0.0896	0.0482
PC-8	0.0585	0.0813	0.1046	0.0523
PC-9	0.0649	0.0519	0.0330	0.0956
Preference selection index	0.79	0.79	0.82	0.84
Preference ranking	4	3	2	1

analysis of the ranking order by using PSI method. The following conclusion points are:

1. The physical and mechanical characterizations like voids content (VC); hardness (H); impact strength (IM); flexural strength (FS); density(D) of composite decrease with increment in Gr (0-6 wt%) reinforcement, while the tensile strength and compressive strength of composite show an increasing trend.
2. ZA-27-Gr alloy composites show the predominant wear resistance performance; and with the base alloy at steady-state sliding wear parameters like normal load (10–40N), sliding velocity (1–1.75 m/s); sliding distance (700–2800m) are under study. Hence, it could be broadly utilized for bearing material application.
3. ZA-27-Gr alloy composite of wear rates decreases with increment in sliding velocity (1-1.75 m/s) under the steady-state wear test irrespective of the reinforcement. The wear rate order is ("0 wt% Gr –ZA-27> 2 wt%Gr-ZA-27> 4 wt%Gr-ZA-27 > 6 wt% Gr-ZA-27"). Also, the coefficient of friction increases with increment in filler content (order: 0 wt%Gr-ZA-27> 2 wt% Gr-ZA-27> 4 wt% Gr-ZA-27 > 6 wt% Gr-ZA-27") across the entire of the spectrum of sliding velocity.
4. Gr reinforced with ZA-27 alloy composite of wear rates increases with increment in normal load (10-40 N) under the steady-state wear test irrespective of the reinforcement. The wear rate order is 0 wt% Gr –ZA-27> 2 wt% Gr-ZA-27> 4 wt% Gr-ZA-27 >6wt% Gr-ZA-27"). Also, the coefficient of friction improves with increment in filler content (order: 0 wt%Gr-ZA-27> 2wt% Gr-ZA-27> 4wt% Gr-ZA-27 > 6 wt% Gr-ZA-27") across the entire of the spectrum of normal load.
5. ZA-27/Gr alloy composite of wear rates increases with increment in sliding distance (700-280 m) under the steady-state wear test irrespective of the reinforcement. The wear rate order is (0 wt% Gr –ZA-27> 2 wt%Gr-ZA-27> 4 wt%SiC-Gr-ZA-27 > 6 wt% Gr-ZA-27"). Also, the coefficient of friction improves with increment in filler content (order: 0wt% Gr-ZA-27> 2wt%Gr-ZA-27> 4wt% Gr-ZA-27 > 6wt%SiC-Gr-ZA-27) across the entire of the spectrum of sliding distance.
6. The complete average for (S/N) proportions for specific wear rate of composites was seen as 75.25 db through D-O-E Taguchi method. The entire sequence of the important factors in reducing the wear rate is ordered as (normal load > filler content > sliding velocity > sliding distance). The similar outcomes are confirmed utilizing ANOVA technique at 5% significance level.
7. The priority order of performance criteria's follows the order (TS) ∼ (FS) ∼ (IS) ∼ (CS) ∼ hardness (HVR) > density (D) > voids content (VC) > wear (W) ∼ coefficient of friction.
8. The fabricated alloy composites having an uniformly mixed of base alloy and particulate reinforcement depict better properties, hence ranked highest by PSI method. The analysis of performance via PSI method depicted the ranking order AGR6>AGR4>AGR2>AGR0.
9. The PSI approach can be successfully used to find better composition of composite formulation subjected to conflicting performance criteria.
10. The study of wear data and SEM micrograph of 6 wt% Gr –ZA-27alloy composites show the superior wear performance comparatively to other composites, hence, it fits for tribological material application.

Acknowledgement

The authors acknowledged the Advanced Research Laboratory for Tribology and Material Research Centre of Malaviya National Institute of Technology Jaipur for characterization facilities and other infrastructure support.

Author's Contribution AK contributed to conceptualization, methodology, experimentation, original draft preparation; MK contributed to reviewing and editing for the final draft preparation.

Funding

No funding to declare.

Data Availability

Additional data are available on reasonable request by email to the corresponding author.

Conflict of interest The authors declare no potential conflicts of interest concerning these articles' research, authorship, and publication.

REFERENCES

1. S.S. Owoeye, D.O. Folorunso, B. Oji, S.G. Borisade, Zinc-aluminum (ZA-27)-based metal matrix composites: a review article of synthesis, reinforcement, microstructural, mechanical, and corrosion characteristics. Int. J. Adv. Manuf. Tech. **100**, 373–380 (2019). https://doi.org/10.1007/s00170-018-2760-9
2. S.C. Tjong, Z.Y. Ma, Microstructural and mechanical characteristics of in situ metal matrix composites. Mater. Sci. Eng. **29**, 49–113 (2000). https://doi.org/10.12691/ijml-1-1-1

3. S.A.B. Raju, K.C. Hemanth, S.I.N. Jayasimha, Mechanical characterization of ZA-27 reinforced with silicon carbide MMC. Proc. Int. Conf. Eng. Sci. Tech. (2017). https://doi.org/10.21647/ICCTEST/2017/48965
4. R. Dalmis, H. Cuvalci, A. Canakci, O. Guler, Investigation of graphite nano particle addition on the physical and mechanical properties of ZA27 composites. Adv. Compos. Mater. **25**(2), 37 (2016). https://doi.org/10.1177/096369351602500202
5. G. Ranganath, S.C. Sharma, M. Krishna, Dry sliding wear of garnet reinforced zinc/aluminium metal matrix composites. Wear **251**, 1408–1413 (2001). https://doi.org/10.1016/S0043-1648(01)00781-5
6. S.C. Sharma, K.H.W. Seah, B.M. Satish, B.M. Girish, Effect of short fibers on the mechanical properties of Cast ZA-27alloy composite. Mater. Des. **17**(6), 245–250 (1996). https://doi.org/10.1016/S0261-3069(97)00016-2
7. K.K. Alaneme, K.O. Adeoye, S.K. Oke, Mechanical and wear behavior of steel chips reinforced ZA27Al composites. Leon. Electro. J. Practices Technol. **29**, 1–16 (2016)
8. B.M. Girisha, K.R. Prakash, B.M. Satisha, Need for optimization of graphite particle reinforcement in ZA-27 alloy composites for tribological applications. Mater. Sci. Eng. A. **530**, 382–388 (2011). https://doi.org/10.1016/j.msea.2011.09.100
9. A. Baradiswaran, A.E. Perumal, Influence of B4C on the tribological and mechanical properties of Al 7075–B4C composites Int. J. Compos. Part B. **54**, 146–152 (2013). https://doi.org/10.1016/j.compositesb.2013.05.012
10. O. Güler, F. Erdemir, M. Çelebi, H. Çuvalcı, A. Çanakçı, Effect of nano alumina content on corrosion behavior and microstructure of ZA27/graphite/alumina hybrid nano composites. Results Phys. **15**, 102700 (2019). https://doi.org/10.1016/j.rinp.2019.102700
11. V. Kumar, G. Gautam, A.K. Yadav et al., Influence of InSitu formed ZrB2 particles on dry sliding behavior of ZA based metal matrix composites. Inter Metalcast (2022). https://doi.org/10.1007/s40962-022-00806-9
12. V. Kumar, G. Gautam, A. Mohan, S. Mohan, Tribology of insitu Zn-Al/ZrB2 composites in reciprocating motion. Int. Metalcast. (2022). https://doi.org/10.1007/s40962-022-00764-2
13. S.J. Huang, M. Subramani, A.N. Ali et al., The effect of micro-SiCp content on the tensile and fatigue behavior of AZ61 magnesium alloy matrix composites. Int. Metalcast. **15**, 780–793 (2021). https://doi.org/10.1007/s40962-020-00508-0
14. M. Shariati, M. Moazami-Goudarzi, A. Abbasi, Microstructure, high-temperature tensile and tribological behavior of Zn/Cr composites. Inter Metalcast (2021). https://doi.org/10.1007/s40962-021-00708-2
15. M. Kumar, S. Bhashkar, N.K. Shakyawal, A. Kumar, Application of preference selection index method in performance (mechanical properties and sliding wear) based ranking of AA2024-Al_2O_3/SiC alloy composites. Materialwiss. Werkstofftech. **51**, 1662–1685 (2020). https://doi.org/10.1002/mawe.201900138
16. A. Vencl, V. Šljivić, M. Pokusová et al., Production, microstructure and tribological properties of Zn-Al/Ti metal-metal composites reinforced with alumina nanoparticles. Inter Metalcast **15**, 1402–1411 (2021). https://doi.org/10.1007/s40962-020-00565-5
17. D. Yousefi, R. Taghiabadi, M.H. Shaeri et al., Enhancing the mechanical properties of Si particle reinforced ZA22 composite by Ti–B modification. Inter Metalcast **15**, 206–215 (2021). https://doi.org/10.1007/s40962-020-00447-w
18. M.A. Maleque, S. Dyuti, M.M. Rahman, Material selection method in design of automotive brake disc. Proc. Worl. Congr. Eng **1**, 2078 (2010)
19. K. Maniya, M.G. Bhatt, A selection of material using a novel type decision-making method preference selection index method. Mater. Des. **31**, 1785 (2010). https://doi.org/10.1016/j.matdes.2009.11.020
20. B.D. Agarwal, L.J. Broutman, *Analysis and performance of fiber composites*, 2nd edn. (John Wiley and Sons Inc, Hoboken, 1990)
21. K. Ravi Kumar, K. Kiran, V.S. Sreebalaji, Characterization of mechanical properties aluminum/tungsten carbide composites. Measurement **102**, 142–149 (2017). https://doi.org/10.1016/j.measurement.2017.01.045
22. S. Santhosh Kumar, M. Devaiah, V. Seshu Bal, T. Rajasekharan, Mechanical properties of SiCp/Al2O3 ceramic matrix composites prepared by directed oxidation of an aluminium. Alloy. Ceram. Int. **38**, 1139 (2012). https://doi.org/10.1016/j.ceramint.2011.08.042
23. S. Gangwar, A. Patnaik, I.K. Bhat, Tribological and Microstructure behavior of quicklime (Cao) filled silicon bronze alloy for bearing material. Silicon **8**, 601–616 (2016). https://doi.org/10.1007/s12633-015-9352-1
24. D. Petkovic, M. Madic, M. Radovanovic, V. Gecevska, Application of the performance selection index method for solving machining MCDM problems. Facta. Univ. Ser. Mech. Eng. **15**, 97–106 (2017). https://doi.org/10.22190/FUME151120001P
25. R. Attri, S. Grover, Application of preference selection index method for decision making over the design stage of production system life cycle. J. King Saud. Univ. Eng. Sci. **27**, 207–2016 (2015). https://doi.org/10.1016/j.jksues.2013.06.003
26. K. Jha, R. Kumar, K. Verma, B. Chaudhary, Y.K. Tyagi, S. Singh, Application of modified TOPSIS technique in deciding optimal combination for biodegradable composite. Vacuum **157**, 259–267 (2018). https://doi.org/10.1016/j.vacuum.2018.08.063
27. R. Khorshidi, A. Hassani, Comparative analysis between TOPSIS and PSI methods of materials

selection to achieve a desirable combination of strength and workability in Al/Sic composite. Mater. Des. **52**, 999–1010 (2013). https://doi.org/10.1016/j.matdes.2013.06.011
28. M. Panahi, H. Gitinavard, Evaluating the sustainable mining contractor selection problems: an imprecise last aggregation preference selection index method. J. Sustain. Min. **16**, 207–2018 (2017). https://doi.org/10.1016/j.jsm.2017.12.006
29. K. Mesran, R.D. Tampubolon, R.D. Sianturi, F.T. Waruwu, Determination of education scholarship recipients using preference selection index. Sci. Tech. **3**, 230–234 (2017). https://doi.org/10.32628/IJSRST173657
30. S.Y. Jian, S.J. Tao, X.R. Huang, Preference selection index method for machine selection in a flexible manufacturing cell. Adv. Mater. Res. **1078**, 290–293 (2014). https://doi.org/10.4028/www.scientific.net/AMR.1078.290
31. H. Abdizadeh, R. Ebrahimifard, M.A. Baghchesara, Investigation of microstructure and mechanical properties of nano MgO reinforced Al composites manufactured by stir casting and powder metallurgy methods: a comparative study. Compos. Part B **56**, 217–221 (2014). https://doi.org/10.1016/j.compositesb.2013.08.023
32. S.C. Sharma, B.M. Girish, R. Kamath, B.M. Satis, Graphite particles reinforced ZA-27 alloy composite materials for journal bearing applications. Wear **219**, 162 (1998). https://doi.org/10.1016/S0043-1648(98)00188-4
33. T. Rajmohan, K. Palanikumar, S. Ranganathan, Evaluation of mechanical and wear properties of hybrid aluminium matrix composites. Trans. Nonferrous Met. Soc. **23**, 2509 (2013). https://doi.org/10.1016/S1003-6326(13)62762-4
34. A. Baradeswaran, A.E. Perumal, Wear and Mechanical characteristics of Al 7075/Graphite composites. Compos. Part B **56**, 472–476 (2014). https://doi.org/10.1016/j.compositesb.2013.08.073
35. K.R. Kumar, K. Kiran, V.S. Sreebalaji, Micro structural characteristics and mechanical behaviour of aluminium matrix composites reinforced with titanium carbideJ. Alloys Compd **723**, 795–801 (2017). https://doi.org/10.1016/j.jallcom.2017.06.309
36. B.V. Ramnath, C. Elanchezhian, M. Jaivignesh, S. Rajaesh, C. Parswjinan, A. Siddique Ahmed, Evaluation of mechanical properties of aluminium alloy–alumina–boron carbide metal matrix composites. Mater. Desi. **58**, 332–338 (2014). https://doi.org/10.1016/j.matdes.2014.01.068
37. S. Ozden, R. Ekici, N. Nair, Investigation of impact behaviour of aluminium based SiC particle reinforced metal–matrix composites. Compos A Appl S. **38**, 484–494 (2007). https://doi.org/10.1016/j.compositesa.2006.02.026
38. J.U. Ejiofor, R.G. Reddy, Developments in the processing and properties of particulate Al-Si composites. J. Miner. Proc. **49**, 31–37 (1997). https://doi.org/10.1007/s11837-997-0008-5
39. B.P. Krishan, P.K. Rohatgi, Modification of Al–Si alloy melts containing graphite particle dispersions. Meter. Technol. **11**, 41–44 (1984). https://doi.org/10.1179/030716984803274297
40. S. Baskaran, V. Anandakrishnan, M. Duraiselvam, Investigations on dry sliding wear behavior of in situ casted AA7075–TiC metal matrix composites by using Taguchi technique. Mater. Des. **60**, 184–192 (2014). https://doi.org/10.1016/j.matdes.2014.03.074
41. A.K. Mondal, S. Kumar, Dry sliding wear behaviour of magnesium alloy-based hybrid composites in the longitudinal direction. Wear **267**, 458–466 (2009). https://doi.org/10.1016/j.wear.2008.12.036
42. H. Chi, L. Jiang, G. Chen, Dry sliding friction and wear behaviour of (TiB_2 + h-BN)/2024Al composites. Mater. Des. **87**, 960–968 (2015). https://doi.org/10.1016/j.matdes.2015.08.088
43. K. Niranjan, P.R. Lakshmi Narayanan, Optimization of process parameters for in situ casting of Al/TiB2 composites through response surface methodology. Trans. Nonferrous Met. Soc. China **23**, 1269–1274 (2013). https://doi.org/10.1016/S1003-6326(13)62592-3
44. S.A. Alidokhta, A.A. Zadeh, H. Assadi, Effect of applied load on the dry sliding wear behaviour and the subsurface deformation on hybrid metal matrix composite. Wear **305**, 291–298 (2013). https://doi.org/10.1016/j.wear.2012.11.043
45. H.R. Manohara, T.M. Chandrashekharaiah, K. Venkateswarlu, S.A. Kori, Dry sliding wear response of A413 alloy: influence of intermetallics and test parameters. Tribol. Int. **51**, 54–60 (2012). https://doi.org/10.1016/j.triboint.2012.02.023
46. C.S. Ramesh, R. Keshavamurthy, B.H. Channabasappa, S. Promod, Friction and wear behaviour of Ni–P coated Si_3N_4 reinforced Al6061 composites. Tribol. Int. **43**, 623–634 (2010). https://doi.org/10.1016/j.triboint.2009.09.011
47. J.C. Walker, W.M. Rainforth, H. Jones, Lubricated sliding wear behaviour of aluminium alloy composites. Wear **259**, 577–589 (2005). https://doi.org/10.1016/j.wear.2005.01.001
48. E. Naveena, S. Ilangovan, Optimization of hardness and wear parameters of Al-Cu-Si alloy using design of experiments. Mater. Today: Proc. **22**, 2704–2714 (2020). https://doi.org/10.1016/j.matpr.2020.03.401
49. O. Savas, Application of Taguchi's method to evaluate abrasive wear behavior of functionally graded aluminum-based composite. Mater. Today Communi. **23**, 100 (2020). https://doi.org/10.1016/j.mtcomm.2020.100920
50. T. Sathis, S. Karthick, Wear behaviour analysis on aluminium alloy 7050 with reinforced SiC through

Taguchi approach. J. Mater. Sci. Technol. **9**(3), 3481–3487 (2020). https://doi.org/10.1016/j.jmrt.2020.01.085
51. S. Arif, B. jamil, M.B.N. Shaikh, T. Aziz, A.H. Ansari, M. Khan, Characterization of surface morphology, wear performance and modelling of graphite reinforced aluminium hybrid composites. Eng. Sci. Tech. Int. J. **23**, 674–690 (2020). https://doi.org/10.1016/j.jestch.2019.07.001
52. X. Li, M. Sosa, U. Olofesson, A pin-on-disc study of the tribology characteristics of sintered versus standard steel gear materials. Wear **340**, 31–40 (2015). https://doi.org/10.1016/j.wear.2015.01.032
53. T.S. Kran, M.P. Kumar, S. Basarajappa, B.M. Viswanatha, Dry sliding wear behavior of heat treated hybrid metal matrix composite using Taguchi techniques. Mater. Des. **63**, 294–304 (2014). https://doi.org/10.1016/j.matdes.2014.06.007
54. S. Gangwar, V. Payak, V.K. Pathak, A. Jamwal, P. Gupta, Characterization of mechanical and tribological properties of graphite and alumina reinforced zinc alloy (ZA-27) hybrid metal matrix composites. J. Compos. Mater. **54**(30), 4751–4771 (2020). https://doi.org/10.1177/0021998320938442
55. A. Kumar, M. Kumar, B. Pandey, Investigations on mechanical and sliding wear performance of AA7075-SiC/Marble dust/Graphite hybrid alloy composites using hybrid ENTROPY-VIKOR method. Silicon **14**, 2051–2065 (2022). https://doi.org/10.1007/s12633-021-00996-7/2021